

1 Targeting Uropathogenic *Escherichia coli*, a Virulent Stains of Urinary Tract 2 Infection: In Silico Study of *Aloe Barbadosis Miller* Phytoconstituents

3 4 5 6 Abstract

7 The most frequent pathogen linked to the development of UTIs is Uropathogenic *Escherichia coli*
8 (UPEC). Thus, inhibiting the UPEC protein target (PDB ID 8BVD) would be a viable treatment
9 approach. This study used molecular docking and dynamics to investigate *Aloe barbadensis miller*
10 antibacterial activity against UPEC bacteria. The Phytoconstituents of *Aloe barbadensis miller*
11 such as aloe-emodin, cholic acid, and flavonol were downloaded from the PubChem database with
12 nitrofurantoin as a control drug and investigated against the target molecule. Some potential
13 parameters such as docking scores, absorption, distribution, metabolism, excretion, toxicity
14 (ADMET), oral bioavailability, root mean square deviation (RMSD), root mean square fluctuation
15 (RMSF), hydrogen bonding, radius of gyration, and total energy of the system were examined.
16 According to the docking score results, all ligands showed excellent candidacy as an inhibitor of
17 the 8BVD molecule. The score order was aloe-emodin (-6.6 kcal/mol), cholic acid (-6.8 kcal/mol),
18 flavonol (-6.8 kcal/mol) and nitrofurantoin (-6.1 kcal/mol). Every ligand seemed to possess
19 favorable drug-likeness characteristics and oral bioavailability. Molecular dynamics investigation
20 showed that every ligand demonstrated a strong candidate for an inhibitor in its vicinity of 20 ns.
21 Contrary to cholic acid, which appears to be more stable, aloe-emodin and flavonol showed
22 comparatively high fluctuations. The results of this study imply that the chosen Phytoconstituents
23 may be employed as 8BVD protein inhibitors to combat urinary tract infections. Nevertheless, the
24 room is still available for more research to validate the particular mechanism of UTI treatment
25 through clinical and experimental methods.

26
27 **Key words:** Molecular docking, Molecular dynamics, Phytoconstituents, Uropathogenic
28 *Escherichia Coli*, Virulent Strain.

29 30 Introduction

31 Urinary tract infection (UTI) is the most prevalent infectious disease identified worldwide,
32 particularly in many developing countries (Mwang'onde & Mchami 2022). It is one of the
33 predominant microbial disorders in clinical practice. Approximately 150 million people are
34 believed to have UTIs globally with significant morbidity and high medical costs per annum
35 (Zagaglia et al., 2022). The annual societal costs of these infections in the USA alone are estimated
36 to be around US dollar 3.5 billion, including medical expenses and lost productivity (Flores-
37 Mireles et al., 2015). Most of the population visiting healthcare facilities, especially those in
38 developing and middle-income countries, perceived the disease more often. This includes
39 schoolchildren, students in higher learning institutions, and any member of the public, mostly
40 women living in communal camps or organizations. There are two clinical classifications for UTIs;
41 complicated and non-complicated types. "Several factors that impair the urinary tract or host
42 defense have been connected to complicated UTIs including immunosuppression, renal failure,
43 pregnancy, urinary blockage, urine retention, and indwelling catheters or other drainage, while

44 non-complicated UTIs were associated with the health of patients showing the absence of
45 structural or neurological urinary tract abnormalities” (Flores-Mireles et al., 2015 & Zagaglia et
46 al., 2022).

47
48 Uropathogenic *E. coli* (UPEC) is a major cause of UTIs leading to a significant burden on public
49 health (Mousavifar et al., 2023). UPEC are the most commonly isolated bacteria globally
50 accounting for 80 to 90%, compared to other gram-negative and gram-positive bacteria (Terlizzi
51 et al., 2017, Seifu & Gebissa 2018, Mwang’onde & Mchami 2022). “The bacteria have **stains** that
52 change from their commensal state as intestinal flora develop and remain in the urinary tract, and
53 exhibit a wide range of virulence factors and tactics, allowing them to infect and cause illnesses in
54 the urinary tract” (Shah et al., 2019).

55
56 Antibiotics such as nitrofurantoin, β -lactams, trimethoprim, and quinolones have been used as
57 routine treatments of UTIs in many developing countries. Although some of these medications
58 have been shown to be effective in reducing the clinical symptoms of UTIs, recurring and chronic
59 infections still affect many individuals (Asadi Karam et al., 2019). “Phytochemicals derived from
60 natural products have been used in drug development, and these products have been considered in
61 the chase for the novel medication combined with other strategies like computational method”
62 (Yuan et al., 2016).

63
64 “Computational methods of molecular docking and dynamics are effective for identifying new
65 drugs and are thus widely used in the pharmaceutical industry” (Fatriansyah et al., 2022).
66 “Computer-aided drug discovery and design may shorten the time taken for a medicine to reach
67 the consumer market, in addition to lowering the expenses involved in drug discovery by
68 guaranteeing that the best lead molecule can enter animal trials” (Preman et al., 2022).

69
70 “Medical plants with antibacterial and anti-inflammatory qualities have been used recently to treat
71 a wide range of infectious diseases in humans” (Fialová et al., 2021). “Aloe vera (*Aloe barbadensis*
72 *miller*) is a well-known therapeutic plant used against UPEC” (Goudarzi et al., 2018). “Its
73 phytoconstituents have major pharmacological features and are widely recognized for their
74 numerous health benefits including its ability to boost immunity, reduce inflammation, prevent
75 sunburn, age prematurely, and anti-cancer”. (Maan et al., 2018). “As a result, they are becoming
76 increasingly popular among clinical researchers as a way to provide cost- and time-efficient
77 therapeutic options for eradicating UTIs” (Goudarzi et al., 2018 & Newman and Cragg 2020).

78
79 Therefore, this study used computational methods to ascertain the antibacterial properties of aloe-
80 emodin, cholic acid, and flavonol derived from *Aloe barbadensis miller* and nitrofurantoin as
81 control drugs. Molecular docking and dynamic studies were conducted to evaluate important
82 parameters such as docking score, hydrogen bond, root mean square deviation (RMSD), root mean
83 square fluctuation (RMSF) radius of gyration, and total energies of the system.

84

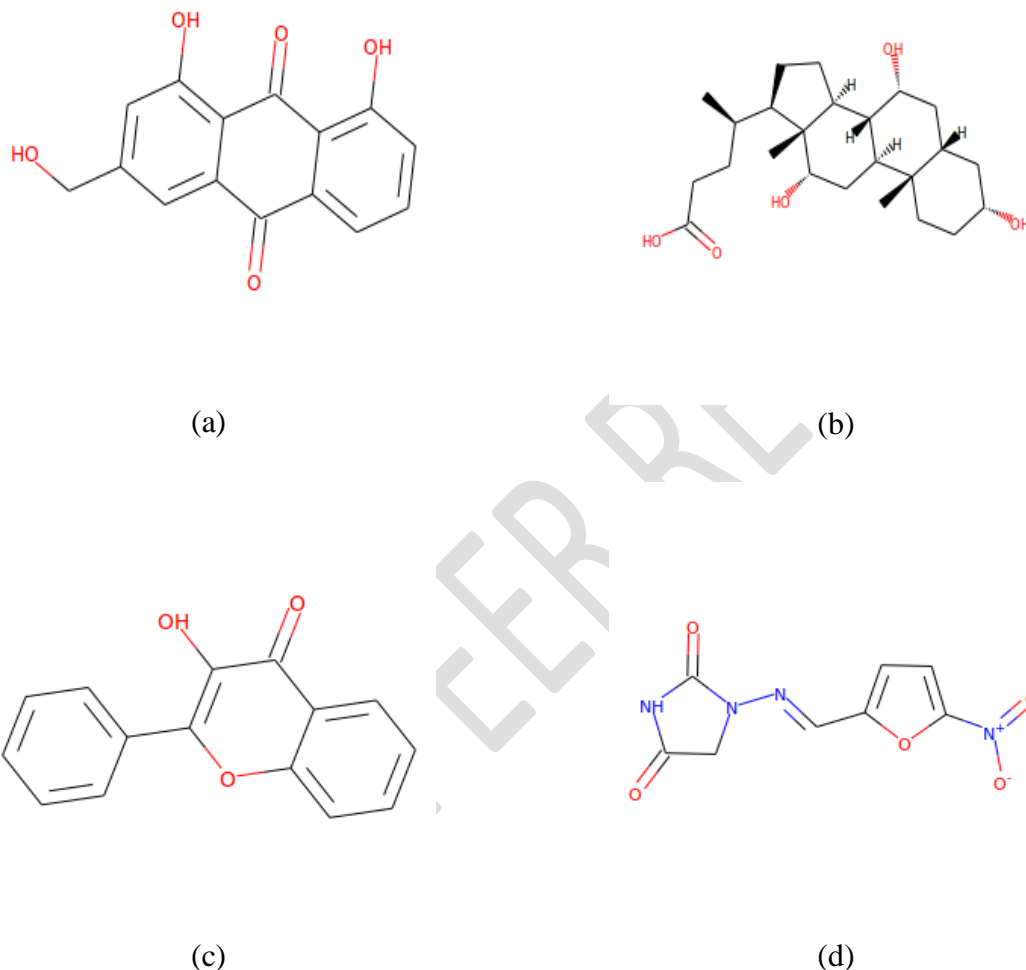
85 **Materials and Methods**

86

87 *Materials Collection*

88

89 The structures of aloe-emodin, cholic acid, flavonol, and nitrofurantoin were downloaded from the
90 PubChem library as 3D conformers and saved as a structure data file (sdf) (Kim et al., 2023). Their
91 molecular structures are shown in (Figure 1).



92 **Figure 1.** Molecular structures of the compounds (a) aloe-emodin, (b) cholic acid, (c) flavonol and (d) nitrofurantoin

93
94 *Protein Selection and Preparation*

95
96 “The protein molecule UPEC type 1 fimbrial (FimH) lectin domain in complex with mannose C-
97 linked to quinolone was downloaded from Protein Data Bank (PDB ID: 8BVD)” (Mousavifar et
98 al., 2023). “Using the X-ray diffraction method the desired macromolecule was obtained with a
99 resolution of 3.00 Å an R-value free of 0.303 and an R-value work of 0.251, indicating good quality
100 and high resolution of the molecule” (Kleywegt & Jones, 1997). “UPEC type 1 FimH complex
101 molecules are desirable substitutes for antibiotic therapy and prophylactic measures against acute
102 or urinary tract infections” (Abe et al., 2008 & Mousavifar et al., 2023). Protein receptors were
103 prepared using the Usf Chimera software by removing solvent and ligand molecules from the
104 8BVD target, removing residues selenomethionines to methionine’s, adding hydrogen atoms, and

105 charging the protein for protein optimizations. (Gurisha et al., 2024). For site-specific docking, the
106 ligand coordinates for the center at X: 26, Y: 58, Z: -9, and box with dimensions of X: 13, Y: 7,
107 and Z: 10 were designed. The ready-to-dock protein receptor was saved in the mol2 file.

108

109 *Ligand Preparations*

110

111 The Phytoconstituents of *Aloe barbadensis miller* were recovered from the commercial PubChem
112 library that was easily accessible. The ligands were prepared using Ucsf Chimera software, which
113 optimized them to match the protein and saved the results as mol2 in the working directory
114 (Pettersen et al., 2004).

115

116 *Molecular Docking*

117

118 Docking is a computational technique that forecasts the interaction between small molecules
119 (ligands) and proteins (enzymes). The program's score function analyzes the docking results; a
120 lower value indicates a better interaction (Stanzione et al., 2021). Molecular docking was
121 performed using Ucsf chimera software that can be expanded upon to facilitate the interactive
122 conception and investigation of molecular structures and associated data. This includes sequence
123 alignments, density maps, conformational ensembles, docking results, trajectories, and
124 supramolecular assemblies (Pettersen et al., 2004).

125

126 “The protein receptor and the minimized ligand saved in the mol 2 file were selected and opened
127 in the auto dock vina window. The receptor and ligand were selected as outputs, and the
128 coordinates for the center and the size for site-specific docking were generated in the boxes. The
129 executable location path for the vina and vina splits was set and docking was performed”. [17]

130

131 *Physicochemical, Pharmacokinetics, Drug-Likeness and ADMET Prediction*

132

133 The pharmacokinetic and pharmacodynamic profiles of a drug are largely determined by its
134 physicochemical qualities, which are crucial for boosting a drug candidate's chances of success
135 during the preclinical development process (Camp et al., 2015). Drug candidates fail in clinical
136 trials for a variety of reasons, but the two main reasons are undesirable pharmacokinetic
137 characteristics and unacceptable toxicity (Honorio et al., 2013). Drug candidates must thus be
138 chosen carefully by researchers to ensure that effectiveness, absorption, distribution, metabolism,
139 excretion, and toxicity are all balanced (Yang et al., 2019). On the other hand, certainly, the
140 inhibition of these isoenzymes (CYP1A2, CYP2C19, CYP2C9, CYP1A2, CYP2D6, and
141 CYP3A4) contributes to pharmacokinetics. Related drug-drug interactions can result in toxic or
142 other unfavorable side effects because of the reduced clearance and buildup of the drug or its
143 metabolites. In this study, the three best-scoring ligands were evaluated: physicochemical,
144 pharmacokinetic (PK), Drug-Likeness and ADMET Prediction using pkCSM and SwissADME
145 web tools (Pires et al., 2015 & Daina et al., 2017).

146

147 *Bioavailability Radar*

148

149 “Drug likenesses are quickly assessed by using bioavailability radar, in this case, six
150 physicochemical parameters like lipophilicity, size, polarity, solubility, flexibility, and saturation

151 were considered” (Udugade et al., 2019). SwissADME software was used to conduct thorough and
152 accurate testing (Diana et al., 2017).

153 154 *Molecular Dynamics*

155
156 “The GROMACS software was used to perform molecular dynamics simulations on 8BVD-
157 CID10207, 8BVD-CID221493, 8BVD-CID11349, and 8BVD-CID6604200 at 300 K with a
158 CHARMM27 force field, and the hybrid ligand structure and force field properties of the chosen
159 ligand were determined using Swiss Param” (Van Der Spoel et al., 2005).

160
161 “Free 8BVD, 8BVD-CID10207, 8BVD-CID221493, 8BVD-CID11349, and 8BVD-CID6604200
162 were solvated with water in a cubic box with a basic diameter of 1 nm with all default settings.
163 Using constant volume and periodic boundary conditions, the system temperature was raised from
164 0 to 300 K throughout the equilibration time (1000 ps). The system was then lowered using the
165 1000 sharpest decline steps. The created trajectories were utilized to evaluate each complex’s
166 behavior as well as the system’s overall stability. Calculations of the hydrogen bond, root mean
167 square deviation, root mean square fluctuation, radius of gyration, and total energies were used to
168 examine the variations in the macromolecule and macromolecule-ligand complex system” (Salaria
169 et al., 2022).

170
171 The equilibration process was divided into two phases using the number of particles, system
172 volume and temperature (NVT) ensemble, and number of particles system pressure and
173 temperature (NPT) ensemble. The C backbone atoms of the original structures were confirmed,
174 while all the other atoms were free to move in both NVT and NPT. Molecular dynamics (MD) was
175 then run at 300k with a 20ns time frame. The GROMACS analysis modules were used to examine
176 the trajectories obtained. UCF Chimera and Maestro were used to visualize MD movies and
177 interaction diagrams, respectively (Walters et al., 2014).

178 179 **Results and Discussion**

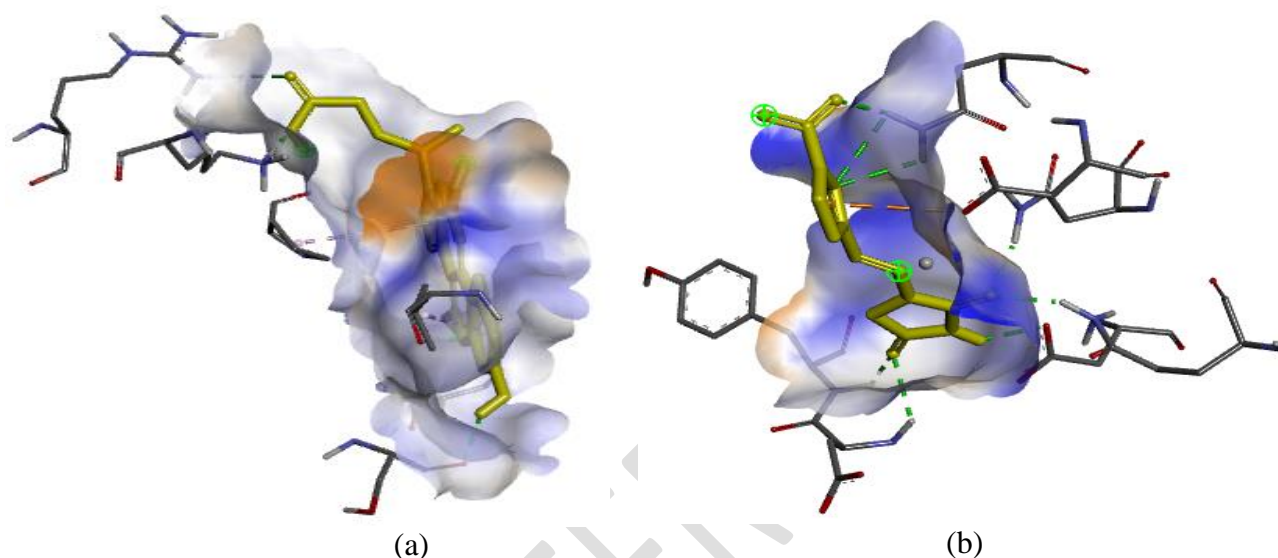
180 181 *Docking Scores*

182
183 Molecular docking scores for aloe-emodin, cholic acid, flavonol, and nitrofurantoin are shown in
184 Table 1. According to the scores, the ligand cholic acid has the lowest affinity for binding to the
185 8BVD target. A lower docking score indicates that ligand and target binding are more stable. The
186 different structures bound to the target caused variations in ligand-target interactions which led to
187 different docking scores (Fatriansyah et al., 2022) (Figure 2). Small molecules of cholic acid have
188 been reported as potential lead drugs for the treatment of bacterial infections (Wu et al., 2023).

189
190
191
192
193
194
195

Table 1. Docking score for ligand-protein target

PubChem ID	Molecular Formula	Name	Docking Scores (kcal/mol)
10207	C ₁₅ H ₁₀ O ₅	Aloe-emodin	-6.6
221493	C ₂₄ H ₄₀ O ₅	Cholic Acid	-6.8
11349	C ₁₅ H ₁₀ O ₃	Flavonol	-6.7
6604200	C ₈ H ₆ N ₄ O ₅	Nitrofurantoin	-6.1



197 **Figure 2.** Visualization of hydrophobic interaction between 8BVD with cholic acid ligand (a) and (b) nitrofurantoin

198

199 *Physicochemical, Pharmacokinetics, Drug-Likeness and ADMET Prediction*

200

201 A molecule needs to have the ideal pharmacokinetics and safety profile in addition to the intended
 202 biological functions to be taken into consideration as a potential therapeutic candidate (Hu et al.,
 203 2018). One of the biggest challenges for oral medicine is its ability to cross the intestinal epithelial
 204 barrier, which affects the rate and degree of human absorption (Rao et al., 2020). The selected
 205 compounds have an intestinal absorption rate of more than 60%, which is extremely high (Table
 206 2). The selected molecules are non-hepatotoxic, do not cause skin sensitization, are non-permeable
 207 to the central nervous system (CNS) and blood-brain barrier (BBB), and exhibit negative AMES
 208 toxicity. It can also be reported that all ligands in this assessment permeate colon carcinoma cell 2
 209 (CaCo-2) although aloe-emodin seems to have a low penetration potential.

210

211 The metabolic enzyme cytochrome P450 (CYP450) was examined and tested in the context of
 212 metabolism. The results indicating that, aloe-emodin and flavonol are potential inhibitors of
 213 CYP1A2, CYP1A2, and CYP3A4. Every ligand was also examined for toxic risks, such as
 214 hepatotoxicity, and the findings demonstrated that none of the substances could harm or impair
 215 the liver (Figure 2). The combination of the drug-likeness and ADMET properties suggested that
 216 aloe-emodin, flavonol, and cholic acid could be good options to inhibit the target in UTI drug
 217 development. According to the available data, aloe-emodin has a wide range of pharmacological
 218 effects such as anti-inflammatory, antibacterial, neuroprotective, hepatoprotective, and anti-tumor

219 effects (Dong et al., 2020). Cholic acid has been described to exhibit antibacterial, anti-viral, anti-
 220 fungal, anti-malaria, anti-tubercular, anti-tumor, and anti-allergic. It is a useful building block that
 221 can be used to create new molecules and a variety of compounds (Kishua & Siva, 2010).
 222 **Flavonol** is a ketone group of flavonoid (Panche et al., 2016). They are considered antioxidant,
 223 anti-mutagenic, anti-inflammatory, and anti-carcinogenic. In addition to these abilities, they also
 224 alter the activities of important cellular enzymes (Burak & Imen, 1999).

225 **Table 2:** ADMET prediction of the highest scoring Phytoconstituents

Properties	Model name	Predicted Value				Unit
		CID 10207	CID 221493	CID 11349	CID 6604200	
Absorption	Water solubility	-3.104	-3.763	-3.683	-2.906	mol/L
	P-gp substrate	No	Yes	No	No	-
	P-glycoprotein	No	Yes	No	No	-
	Gastrointestinal absorption	High	High	High	High	-
	Caco-2 permeability	-0.233	0.597	1.263	-0.013	cm/s
	Intestinal absorption(%)	74.179	61.546	94.776	79.533	-
Distribution	BBB permeability	-0.729	-0.716	0.462	-0.9	Log BB
	VDss (human)	0.671	-0.804	0.214	-0.544	Log L/kg
	Fraction unbound	0.226	0.171	0.151	0.54	Fu
	CNS permeability	-	-2.344	-1.733	-3.18	Log Ps
Metabolism		0.2466				
	Leadlikeness	Yes	No	No	No	-
	Inhibitor CYP1A2	Yes	No	Yes	No	-
	CYP2C19	No	No	Yes	No	-
	CYP2C9	No	No	No	No	-
	CYP2D6	No	No	Yes	No	-
	CYP3A4	Yes	No	Yes	No	-
Excretion	CYP1A2	Yes	No	Yes	No	-
	Total Clearance	0.008	0.653	0.233	0.665	ml/min/kg
	Renal OCT2 substrate	No	No	No	No	-
Toxicity	Skin sensitization	No	No	No	No	-
	Hepatotoxicity	No	No	No	No	-
	AMES toxicity	No	No	No	Yes	-

227
 228
 229
 230
 231
 232
 233
 234
 235
 236
 237

238
239
240
241

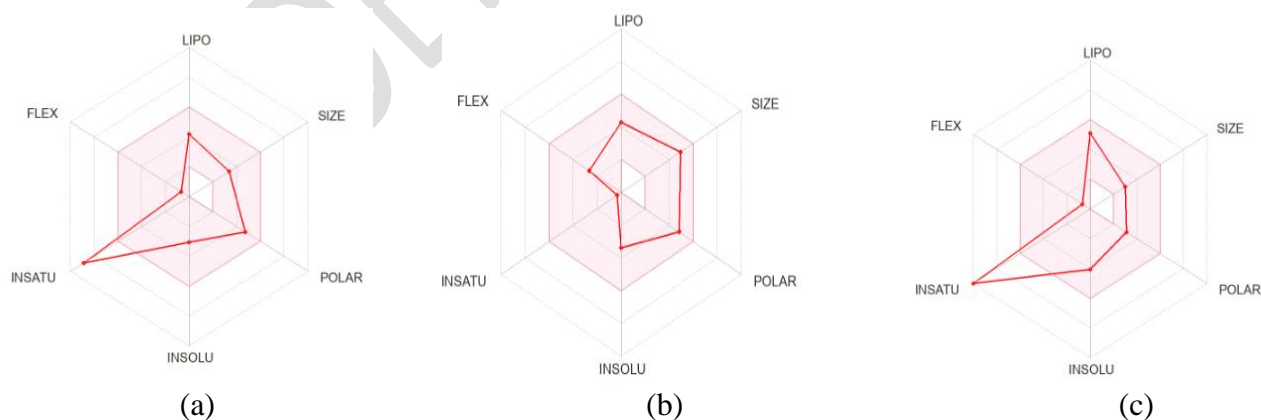
Table 3: Phytoconstituents and drug-like properties analysis

Descriptor/Properties	Value				Units
	CID 10207	CID 221493	CID 11349	CID 6604200	
Molecular Weight	270.24	408.6	238.24	238.16	g/mol
Monoisotopic Mass	270.052826	408.287567	238.062994	238.033813	Da
Rotatable Bonds	1	4	1	3	-
H. Acceptors	5	5	3	6	-
H. Donors	3	4	1	1	-
LogP	1.3655	3.4487	3.1656	0.0735	-
Num. arom. heavy atoms	12	0	16	5	-
Fraction Csp3	0.07	0.96	0.0	0.12	-
Num. of heavy atoms	20	29	18	17	-
Topological Polar Surface Area	94.83	97.99	50.44	120.73	Å ²
Molar Refractivity	69.92	113.76	69.94	62.8	-

242
243
244
245
246
247
248
249
250
251
252
253
254

Bioavailability Radar

A molecule's radar plot needs to fall inside the colored zone to be considered drug-like (Figure 3). For each variable, the pink zone indicates the proper range, such as lipophilicity: XLOGP3 range between -0.7 to 5.0, molecular weight (Mw) ranges between 150 and 500 g/mol, topological polar surface area (TPSA) ranges between 20 and 130 Å², solubility: logS less than 6, saturation (INSATU): fraction csp3 hybridization fraction greater than 0.25, and flexibility: less than 9 rotatable bonds (Table 3). Therefore, based on the bioavailability radar indicated in Figure 3, cholic acid has oral bioavailability, while aloe-emodin and flavonol appear to be more unsaturated with respect to carbon percentage in sp³ hybridization.



255

Figure 3: Bioavailability radar of (a) aloe-emodin, (b) cholic acid and (c) Flavonol

256 To conduct visual analysis, the positions for every ligand-target interaction were compared. To
257 facilitate ligand interactions, the protein active sites were created. Initially, the analysis of the aloe-
258 emodin-target, in which its 2D projection interaction is displayed in Figure 4(a), was deliberated.
259 The three OH groups in aloe-emodin form hydrogen bonds with protein residues Asp47, Asp54,
260 Asp140, Gln133, and Phe1. In this case, aloe-emodin acts as a hydrogen donor to the polar residues
261 Asn54 and Asp140, whereas it acts as an acceptor to the amino acid residues Asp47, Gln133, and
262 Phe1. The bond formed here is somewhat complicated, where aloe-emodin acts as a hydrogen
263 donor and acceptor simultaneously

264
265 The second pose is the cholic acid-target interaction, as displayed in Figure 4(b). The figure shows
266 that cholic acid forms two OH groups in the form of hydrogen bonds with Asp140, and two oxygen
267 bonds with Asp47 and Phe1. In this case, the Asp140 polar residue acts as a hydrogen acceptor,
268 while the amino acid residues Asp47 and Phe1 act as donors to cholic acid oxygen atoms. It is
269 estimated that the docking score of cholic acid is more negative than that of aloe-emodin owing to
270 the interaction of two hydrogen bonds with the Asp140 polar residue.

271
272 The third pose is the flavonol-target interaction, as displayed in Figure 4(c). The figure illustrates
273 that flavonol forms one OH group in the form of a hydrogen bond with Asp140 and one oxygen
274 bond with Asn138. In this case, the Asp140 polar residue acts as a hydrogen bond acceptor,
275 whereas Asn138 acts as a donor to a flavonol oxygen atom. In this situation, the docking score of
276 flavonols seems to be more negative than that of aloe-emodin.

277
278 The fourth pose is the nitrofurantoin-target interaction, as displayed in Figure 4(d). This figure
279 indicates that nitrofurantoin forms a hydrogen bond with Asp54 and an oxygen bond with Asp47,
280 Asn135, Gln133, and Tyr48. In this case, the Asp54 polar residue acts as a hydrogen acceptor,
281 while Asp47, Asn135, Gln133, and Tyr48 act as donors to a nitrofurantoin oxygen atom. In this
282 phenomenon, the docking score of nitrofurantoin appears to be less negative than flavonol
283 compounds.

284
285 In general, the complexity of protein-ligand interactions determines the strength of molecular
286 docking (Madeddu et al., 2022). Aloe-emodin has hydrogen bonds with Asp47, Asp54, Asp140,
287 Gln133, and Phe1 which are more complicated than those of cholic acid, which has two hydrogen
288 bonds with Asp140, flavonol, and nitrofurantoin, which have a single hydrogen bond with Asp140
289 and Asp54, respectively. Therefore, from the visual analysis, the best compound to form a ligand
290 target was cholic acid, followed by flavonol, aloe-emodin, and nitrofurantoin, which were
291 endorsed by the protein-ligand interaction docking scores (Table 1).

292
293 Nitrofurantoin has become the first-line drug choice for the treatment of uncomplicated UTIs in
294 light of updated guidelines, and its use has skyrocketed since then (Mahdizade et al, 2023). From
295 the docking results, nitrofurantoin has a more positive value of the docking score compared with
296 the other three ligands although both have good hydrogen bond interactions. Having the more
297 negative value of the docking scores of aloe-emodin, cholic acid, and flavonol suggests that they
298 might be a suitable candidate for the treatment of UTIs in comparison with the control drug.

299
300
301

302
 303
 304
 305
 306

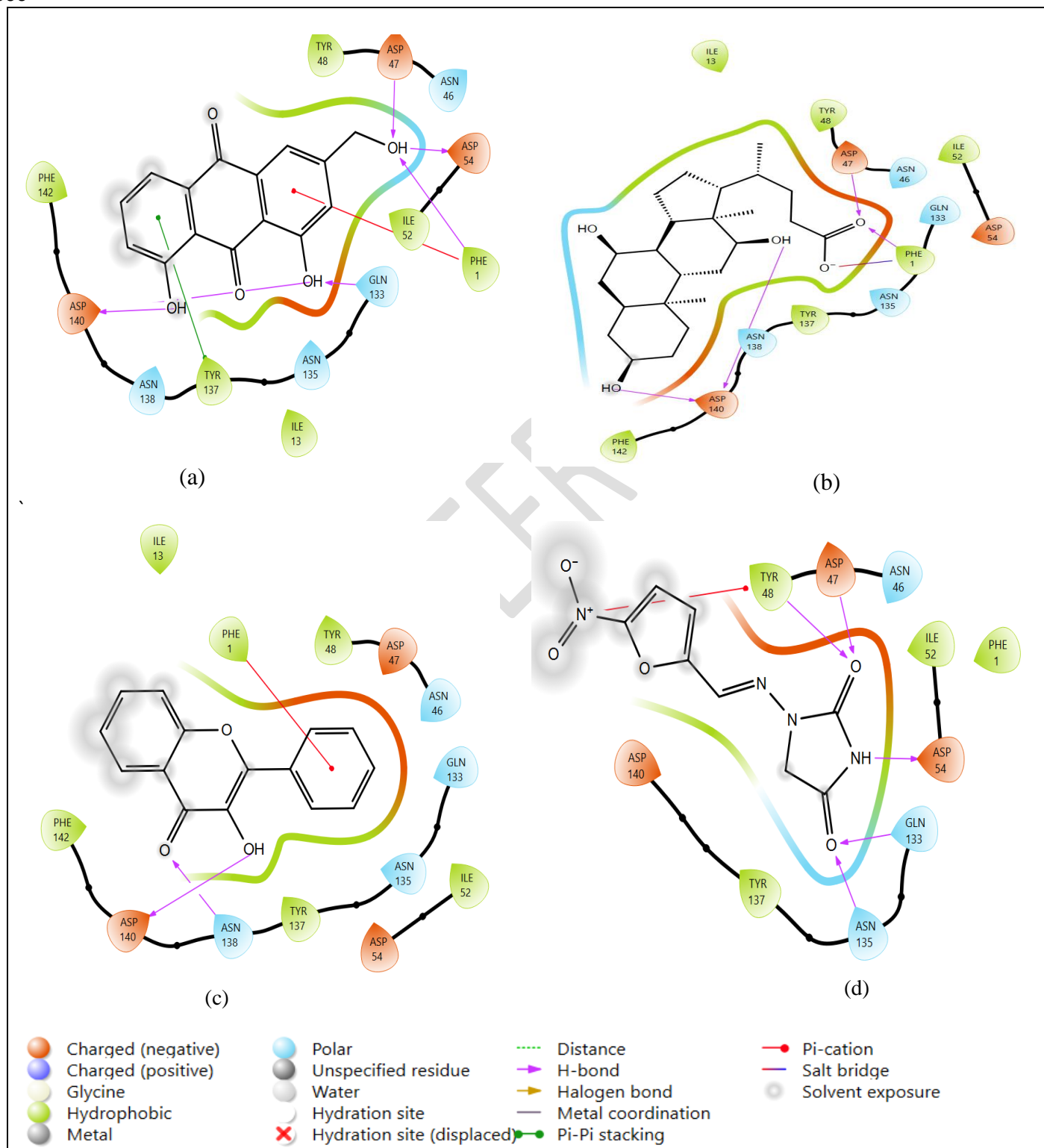
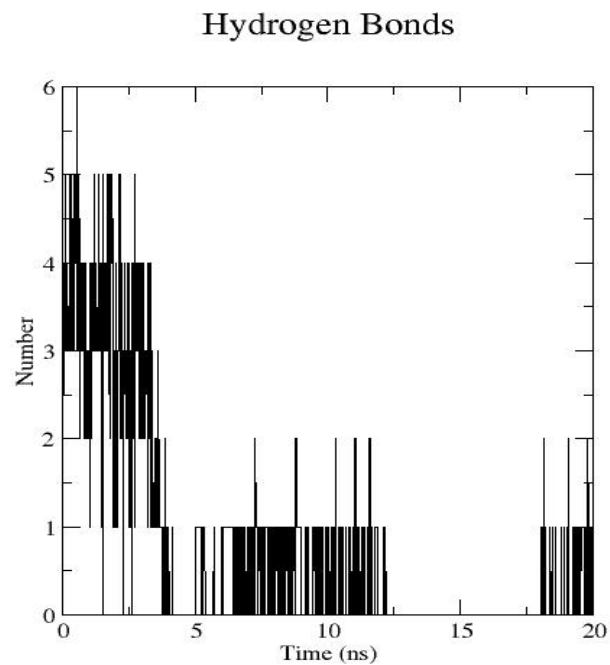
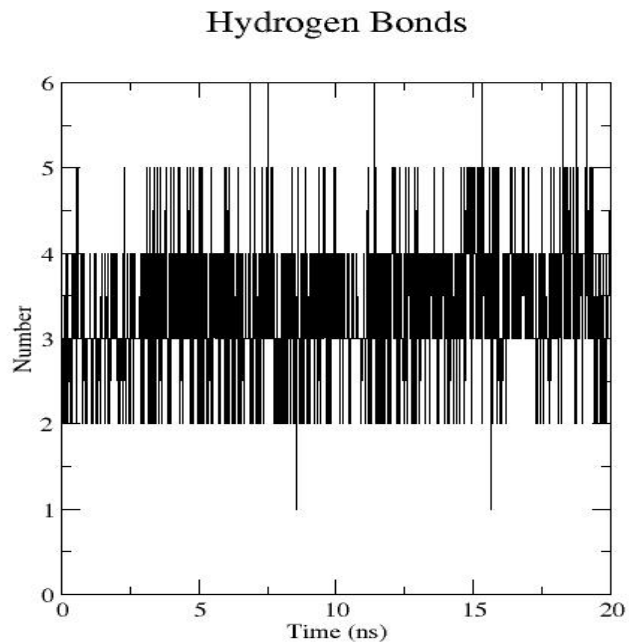


Figure 4. Two-dimension interaction diagrams in various possess within the binding pocket 8BVD for (a) aloec-emodin, (b) cholic acid, (c) flavonol and (d) nitrofurantoin

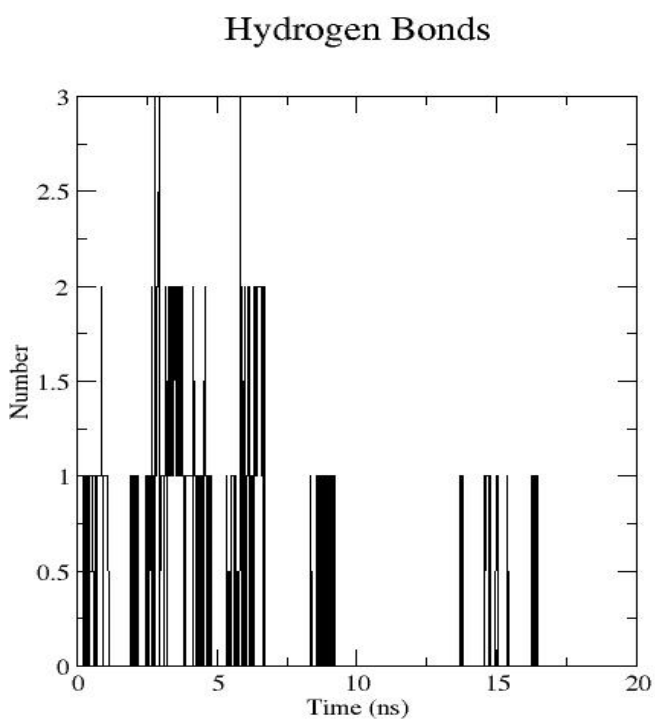
307
308 *Molecular Dynamics*
309
310 Molecular dynamics is a computer modeling technique that forecasts the motion of each atom in a
311 protein or other molecular system over time (Karplus & Mc Cammon 2002). It provides an
312 overview of the system dynamics evolution.
313 Molecular dynamics (MD) was performed to examine the actual motion of atoms, which aids in
314 understanding the detailed interaction of 8BVD with potential phytochemicals, especially when it
315 binds to a protein target (Hansson et al, 2002). Several non-identified biological activities and
316 intricate dynamic processes can be discovered by observing the internal dynamics of proteins
317 (Anwer et al., 2015).
318
319 *Hydrogen Bonding (H-Bonds) Analysis*
320
321 The stability of a protein's three-dimensional structure is mostly determined by intramolecular
322 hydrogen bonding within the protein molecule (Hubbard et al., 2001). Hydrogen bond analysis can
323 also be used to examine the strength of the protein-ligand complex to assess the molecular
324 recognition, directionality, and specificity of contacts (Mohammad et al., 2020). The analysis
325 showed that aloec-emodin formed a maximum of 6-H bonds during the molecular dynamics
326 computation. It was observed that aloec-emodin binds to the active pocket of 8BVD with many H-
327 bond breakages from five to six H- bonds. From 0 to 4 ns, 1 to 5 hydrogen bonds were formed
328 with bond breaking. From 5 to 13 ns, there were one to two stable H-bonds with fluctuations,
329 followed by bond breaking from 13 to 18 ns. Again, from 18 to 20 ns, stable hydrogen bonds were
330 formed, with some fluctuations (Figure 5 a).
331
332 Cholic acid formed a maximum of six H-bonds during the molecular dynamic computation. From
333 8 to 16 ns, a 1–2 H-bond was formed by bond breaking. From 0 to 20 ns, cholic acid bound to the
334 active pocket of 8BVD and formed two to four H-bonds, which were the most stable, although
335 there were some fluctuations. Stable H-bonds were formed between 4 and 5.



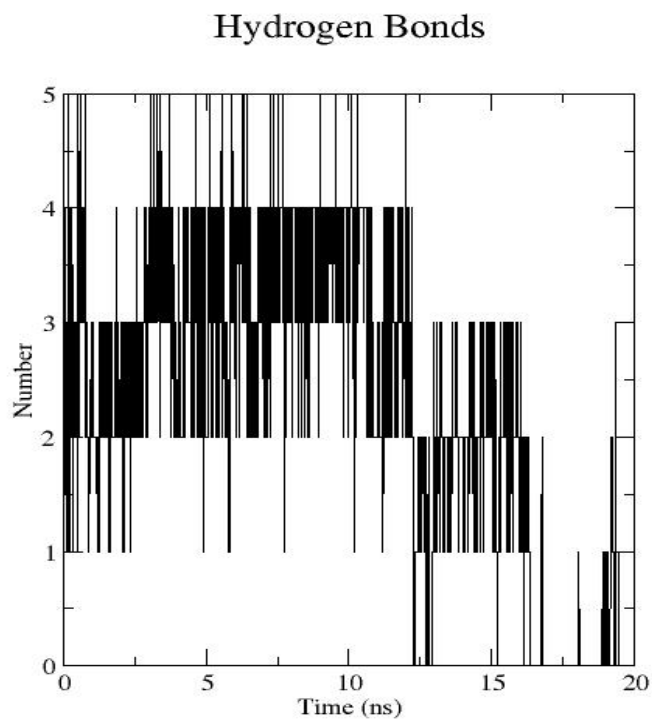
(a)



(b)



(c)



(d)

Figure 5. Hydrogen bonds formed by (a) aloe-emodin (b) cholic acid (c) flavonol and (d) nitrofurantoin

336
337
338
339
340

Hydrogen bonds with high fluctuations compared to the H-bonds formed between 2 two four H-bonds. Equally, from 5 to 6, hydrogen bonds were formed with bond breaking (Figure 5 b).

341
342 Molecular dynamics analysis revealed that flavonol binds to the active pocket of 8BVD and forms
343 a 3 H-bonds. From 0 to 1ns, 0.5 to 2 H-bonds were formed, with some bond breakage. Equally,
344 0.5 to 3 H-bonds were formed with fluctuations and bond breakage from 2 to 7 ns. From 9 to 16
345 ns there a 0.5 to 1 hydrogen bond was formed with bond breakage (Figure 5 c).

346
347 Nitrofurantoin was observed to form a maximum of five H-bonds during the molecular dynamic
348 simulation. From 12 to 20 ns, nitrofurantoin formed a 1H-bond with fluctuations and bond
349 breakage. Similarly, 1 to 2 H-bonds were formed with some fluctuations and bond breakage,
350 especially from 2 to 12 ns and 16 to 20 ns. Nitrofurantoin formed stable hydrogen bonds from two
351 to four H-bonds with fluctuations and bond breakage, especially from 12 to 20 ns. Other hydrogen
352 bonds were formed between four and five H-bonds with high fluctuations and bond breakage,
353 particularly from 12 to 20 ns (Figure 5 d). Primarily, all four ligands had good H-bonding with the
354 active pocket 8BVD; however, cholic acid had the most stable H-bonding in comparison to other
355 ligands. Protein-ligand binding is highly influenced by H-bonding (Wade RC & Goodford 1989).
356 Therefore, cholic acid has excellent potential for use as a drug candidate.

357
358 *Root Mean Square Deviation (RMSD)*

359
360 The root mean square deviation of each trajectory record for 20 ns in the MD simulation with
361 regard to the initial position of the protein ligand was measured to assess the stability of the docked
362 complex (Anusuya et al., 2015). The mean RMSD for aloe-emodin was 2.32 nm. The plot showed
363 that aloe-emodin binds effectively more stable with 8BVD at 0.99 nm from 0 to 12 ns, and then
364 destabilized at 13 ns to 18 ns.

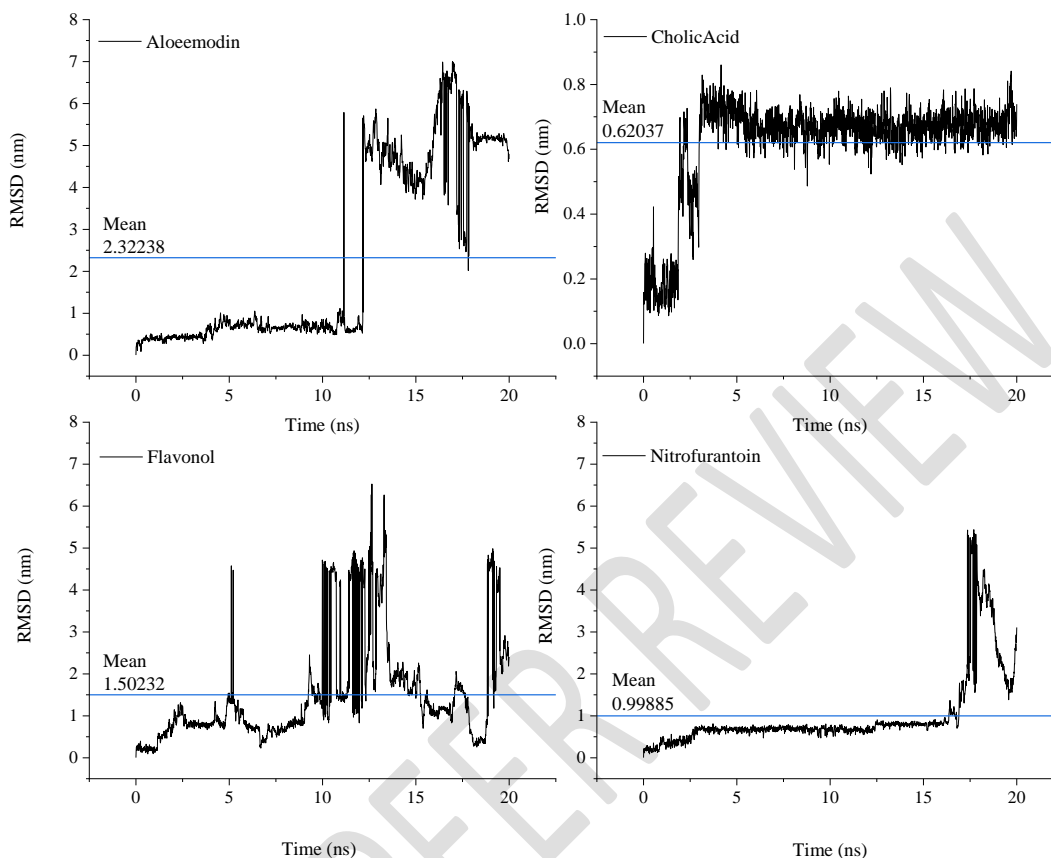


Figure 6. RMSD for aloe-emodin, cholic acid, flavonol and nitrofurantoin ligands

From the trajectory analysis, cholic acid appeared to bind more strongly with the target molecule at 0.8 nm. Initially, the ligand had a slight destabilization from 0–3 ns before stabilizing at 0.35 ns. The mean root mean square deviation (RMSD) was 0.620 nm.

The flavonol ligand was stable from 0–4 ns, before fluctuating at 5 ns. From 5.5 to 9.5 ns the ligand was re-stabilized, but then destabilized from 10 to 13 ns before gaining stability at 18 ns. The mean RMSD value was recorded at 1.50 nm.

RMSD for nitrofurantoin ligands was stable at 0.89 nm from 0 to 17 ns, and then destabilized from 18 ns up to 20 ns. The mean RMSD was recorded at 0.99 nm. Looking at their ranges, cholic acid had the lowest range followed nitrofurantoin, flavonol and aloe-emodin (Figure 6).

385 *Root Mean Square Fluctuation (RMSF)*

386

387 The flexibility of each amino acid residue, or how much it shifts or fluctuates throughout a
388 simulation, was measured by root mean square fluctuation (RMSF), which averages the number
389 of atoms to determine how far an atom or group of atoms has deviated from the reference structure.
390 According to Fatriansyah et al. (2022), stable structures have lower RMSF values. The fluctuation
391 of different atoms was observed for 20 ns, to predict the stable structure, and the RMSF was
392 computed using the GROMACS standard function. The analysis shows that the H10 atom of alo-
393 emodin fluctuated more than the other atoms. The RMSF value of the H10 atom was 0.151 nm,
394 followed by HC5 and HC6, both with RMSF value of 1.121 nm. O5, H8, and H9 atoms fluctuated
395 at an RMSF value of 0.102 nm while the HO atoms fluctuated at 0.7 nm. The other atoms were
396 stable at an average RMSD value of 0.03 nm (Figure 7 a).

397

398 The HC31 atom of cholic acid was perceived to have the highest fluctuation at an RMSF value of
399 0.186 nm, followed by HC32 and HC30 with RMSF values of 0.183 and 0.182 nm, respectively.
400 O5, C22, and HC23 exhibited RMSF values of 0.14, 0.13 and 0.13 nm respectively. The other
401 atoms are stable at an average RMSF value of 0.065 nm (Figure 7 b).

402

403 For the case of flavonol, the HC7 atom seems to have a higher fluctuation at an RMSF value of
404 0,225 nm followed by HC8 fluctuating at 0.221 nm. Both HC4 and HC5 fluctuated at the RMSF
405 value of 0.212 nm while C14 fluctuated at 0.151nm. C10 fluctuated at the RMSF value of 0.150
406 nm followed by C9 and C13 both fluctuated at 0.149 nm. Other atoms are stable at an average
407 RMSF value of 0.499 nm. (Figure 7 c)

408

409 In the case of nitrofurantoin, the HC7 atom had a higher fluctuation with an RMSF value of 0.209
410 nm, followed by HC8, HC4, and HC5 atoms with RMSF values of 0.207, 0.205, and 0.204 nm,
411 respectively. In contrast, atoms such as C14, C13, C9, C10, and H10 also fluctuated, with RMSF
412 values of 0.125, 0.123, 0.122, 0.123, and 0.121 nm, respectively. The other atoms appear to be
413 stable at an average RMSF value of 0.320 nm (Figure 7 d). Most of the atoms observed to have
414 higher RMSF values were terminal atoms.

415

416

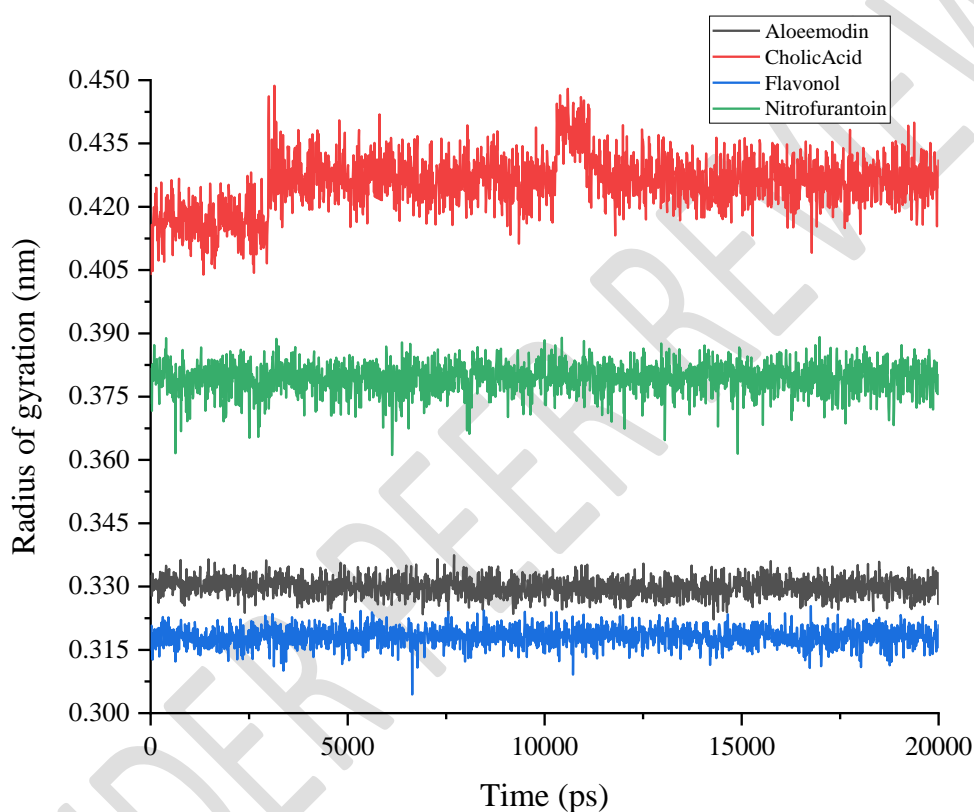
417

420

421 *Radius of gyration (Rg)*

422

423 The compactness of a protein structure is determined by its radius of gyration. In the protein-ligand
424 complex, the radius of gyration of a ligand shows the ligand center of gyration to the center of
425 gyration of the protein; therefore, a higher value of the radius of gyration indicates less stability of
426 the structure (Lobanov et al., 2008). From the analysis, it was observed that cholic acid gyrated
427 more, with a higher value of 0.435 nm. This higher value is attributed to the higher molecular
428 weight of cholic acid which is 408.6 g/mol and the complex shape of the ligand (Alfred & Choi
429 2013).



430

431 **Figure 8.** Radius of gyration for aloe-emodin, cholic acid, flavonol and nitrofurantoin ligands

432

433 Flavonol had the lowest Rg value of about 0.315 nm at 20 ns. The ligand gyrated with this lower
434 value because of the simple structure of flavonol and its lower molecular weight compared to
435 cholic acid. Other ligands such as aloe-emodin and nitrofurantoin have a minimum value of Rg
436 ranging from 0.330 to 0.380 nm respectively at 20 ns (Figure 8).

437

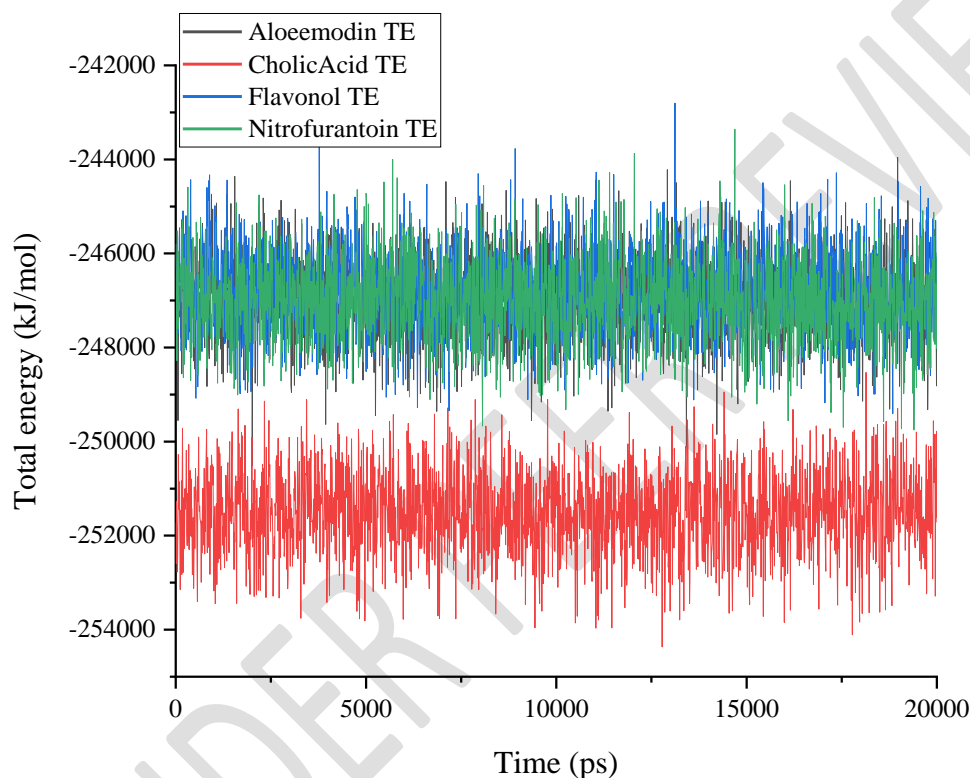
438 *Total Energies of the System*

439

440 The quality and stability of the molecular dynamic simulations were also evaluated through
441 a qualitative investigation of the thermodynamic properties, such as the total energies and
442 temperature (Anwer et al., 2015). The temperature fluctuation of the trajectory was almost

443 constant at 300 K, indicating the stable and precise nature of the molecular dynamics
444 simulation. The total energies of the system of both proteins and ligands were plotted as a
445 function of MD simulation time, and the plots are shown in Figure 9.

446
447 The results from the plot illustrate that cholic acid is more stable than the other three
448 ligands, with a total energy of -252000 kJ/mol. Aloe-emodin, flavonol, and nitrofurantoin
449 ligands were also stable, with slightly higher energies ranging from -248000 to -246000
450 KJ/mol. The trajectory profile's lower energy suggests that the system was remarkably
451 stable during the simulation (Lakshmi et al., 2020).
452



453
454 **Figure 9.** Total Energies of the System during the MD simulation
455

456 Conclusion

457
458 UPEC inhibition is an innovative approach for preventing the emergence of UTIs. Natural
459 compounds are the most important source of medicines for the treatment of many diseases
460 (Veeresham 2012). The ligand-target complex presented a good candidate for molecular docking
461 and molecular dynamics. All ligands were superb candidates as 8BVD inhibitors based on the
462 molecular docking scores, ADMET studies, and drug-like characteristics. Docking score ranges
463 were arranged as follows from high to low as follows: cholic acid, flavonol, aloe-emodin, and
464 nitrofurantoin. These results suggest that cholic acid is a more suitable inhibitor than other ligands.
465 Molecular dynamics revealed that all ligands can also serve as excellent inhibitors, although

466 fluctuations in aloe-emodin and flavonol remain high. However, additional studies and tests are
467 required to validate these compounds as 8BVD protein inhibitors.
468

469 Reference

- 470
- 471 1. Abe, C.M.; Salvador, A.; Falsetti, I.N.; Blanco, E.; Blanco, M. (2008). Uropathogenic
472 *Escherichia coli* (UPEC) strains may carry virulence properties of diarrhoeagenic *E. coli*.
473 *FEMS Immunol. Med. Microbiol.*, 52, pg 397–406. DOI: 10.1111/j.1574-
474 695X.2008.00388.x
 - 475 2. Alfred Rudin, Phillip Choi. (2013). *the Elements of Polymer Science & Engineering* (Third
476 Edition), Science Direct, Elsevier Inc.
 - 477 3. Anwer, K., Sonani, R., Madamwar, D., Singh, P., Khan, F., Bisetty, K., Ahmad, F., &
478 Hassan, M. I. (2015). Role of N-terminal residues on folding and stability of C-
479 phycoerythrin: simulation and urea-induced denaturation studies, *Journal of Biomol*
480 *Structure Dynamics*, 33(1), pg 121-133. <https://doi.org/10.1080/07391102.2013.855144>
 - 481 4. Anusuya, S., Velmurugan, D., Gromiha, M.M., (2015). Identification of dengue viral
482 RNA-dependent RNA polymerase inhibitor using computational fragment based
483 approaches and molecular dynamics study. *J. Biomol. Struct. Dyn.* 34 (7), pg 1512–1532.
484 <https://doi.org/10.1080/07391102.2015.1081620>
 - 485 5. Asadi Karam, M. R., Habibi, M., & Bouzari, S. (2019). Urinary tract infection:
486 Pathogenicity, antibiotic resistance and development of effective vaccines against
487 Uropathogenic *Escherichia coli*. *Mol Immunol*, 108, pg 56-67.
488 <https://doi.org/10.1016/j.molimm.2019.02.007>
 - 489 6. Beda John Mwang'onde, Josefina Innocent Mchami.(2022).The aetiology and prevalence
490 of urinary tract infections in Sub-Saharan Africa: a Systematic Review, *J. Health Biol*
491 *Sci.*;10(1):pg 1-7
 - 492 7. Bittner Fialová S, Rendeková K, Mučaji P, Nagy M, Slobodníková L. (2021). Antibacterial
493 Activity of Medicinal Plants and Their Constituents in the Context of Skin and Wound
494 Infections, Considering European Legislation and Folk Medicine-A Review. *Int J Mol Sci.*
495 22(19):10746. doi: 10.3390/ijms221910746.
 - 496 8. Burak M & Imen Y .(1999). Flavonoids and their antioxidant properties. *Turkiye Klin Tip*
497 *Bil Derg* vol 19, pg 296–304.
 - 498 9. Chhaya Shah, Ratna Baral, Bijay Bartaula and Lok Bahadur Shrestha. (2019). Virulence
499 factors of uropathogenic *Escherichia coli* (UPEC) and correlation with antimicrobial
500 resistance, *BMC Microbiology Journal*, 19 (204). [https://doi.org/10.1186/s12866-019-](https://doi.org/10.1186/s12866-019-1587-3)
501 1587-3
 - 502 10. Christopher A Lipinski; Franco Lombardo; Beryl W Dominy; Paul J Feeney.
503 (2001). Experimental and computational approaches to estimate solubility and
504 permeability in drug discovery and development settings, *Advanced Drug Delivery*
505 *Reviews* 46(1-3), pg 3–26. doi:10.1016/s0169-409x(00)00129-0
 - 506 11. Daina, A., Michielin, O. & Zoete, V. (2017).SwissADME: a free web tool to evaluate
507 pharmacokinetics, drug-likeness and medicinal chemistry friendliness of small
508 molecules. *Sci Rep* 7, (42717) <https://doi.org/10.1038/srep42717>
 - 509 12. David Camp, Agatha Garavelas, and Marc Campitelli. (2015). Analysis of
510 physicochemical properties for drugs of natural origin, *J. Nat. Prod.* 78, (6), pg 1370–1382.
511 DOI: 10.1021/acs.jnatprod.5b00255

- 512 13. Dong X, Zeng Y, Liu Y, You L, Yin X, Fu J, Ni J. (2020). Aloe-emodin: A review of its
513 pharmacology, toxicity, and pharmacokinetics. *Phytother Res.* 34(2) pg 270-281. doi:
514 10.1002/ptr.6532.
- 515 14. Douglas E. V. Pires, Tom L. Blundell, and David B. Ascher .(2015). pkCSM: Predicting
516 small-molecule pharmacokinetic and toxicity properties using graph-based signatures,
517 *Journal of medicinal chemistry*, (58) pg 4066–4072.
518 <https://doi.org/10.1021/acs.jmedchem.5b00104>
- 519 15. Flores-Mireles, A.L.; Walker, J.N.; Caparon, M.; Hultgren, S.J.(2015).Urinary tract
520 infections: Epidemiology, mechanisms of infection and treatment options. *Nat. Rev.*
521 *Microbiol*,13, pg 269–284. DOI: 10.1038/nrmicro3432
- 522 16. Gerard J. Kleywegt and T. Alwyn Jones. (1997).Model building and refinement practice.
523 *In Methods in enzymology* (Volume 277, 1997, Pages 208-230).
524 [https://doi.org/10.1016/S0076-6879\(97\)77013-7](https://doi.org/10.1016/S0076-6879(97)77013-7)
- 525 17. Gurisha, M.S., Rao, P.V.K. and Cherupally, L. (2024) Phytochemicals of Aloe barbadensis
526 miller as Potential Inhibitors of Uropathogenic Escherichia coli for Urinary Tract Infection
527 Therapy: An in Silico Approach. *Open Journal of Biophysics*, 14, 99-120.
528 <https://doi.org/10.4236/ojbiphy.2024.142006>
- 529 18. Haidan Yuan, Qianqian Ma, Li Ye and Guangchun Piao.(2016) The traditional medicine
530 and modern medicine from natural products, review, *MDPI Journal of Molecules*, Vol 21,
531 pg 559. DOI: 10.3390/molecules21050559
- 532 19. Hansson, T., C. Oostenbrink, and W. F. van Gunsteren. (2002). Molecular dynamics
533 simulations. *Curr. Opin. Struct. Biol.* vol 12 pg 190–196.
- 534 20. Honório KM, Moda TL, Andricopulo AD. Pharmacokinetic properties and in silico ADME
535 modeling in drug discovery. *Med Chem.* 2013 Mar;9(2):163-76. doi:
536 10.2174/1573406411309020002.
- 537 21. Huang, C.C., Couch, G.S., Pettersen, E.F., and Ferrin, T.E. (1996)."Chimera: an extensible
538 molecular modeling application constructed using standard components." *Pacific*
539 *Symposium on Biocomputing* 1:724
- 540 22. Hubbard, R.E.; Kamran Haider, M. (2001). Hydrogen bonds in proteins: role and strength.
541 *In eLS; John Wiley & Sons, Ltd.:* Hoboken, NJ, USA.
- 542 23. Hu Q, Feng M, Lai L, Pei J. (2018). Prediction of Drug-Likeness Using Deep Autoencoder
543 Neural Networks. *Front Genet.* 27 (9) 585. doi: 10.3389/fgene.2018.00585.
- 544 24. Fatriansyah JF, Rizqillah RK, Yandi MY, Fadilah, Sahlan M. (2022). Molecular docking
545 and dynamics studies on propolis sulabiroidin-A as a potential inhibitor of SARS-CoV-2. *J*
546 *King Saud Univ Sci.* Jan;34(1):101707. doi: 10.1016/j.jksus.2021.101707.
- 547 25. Jia C-Yang, Li J-Yi, Hao G-Fei, Yang G-Fu .(2019). A drug-likeness toolbox facilitates
548 ADMET study in drug discovery, *Drug Discovery Today*
549 <https://doi.org/10.1016/j.drudis.2019.10.014>
- 550 26. J. P. Walters, C. M. Rogers, and S. P. Crago .(2014). Maestro software and application
551 performance, *Conference Paper*, GOMACTech-14 conference.
- 552 27. Karplus M, and McCammon JA (2002). Molecular dynamics simulations of
553 biomolecules. *Nature structural biology* 9, 646–652.
- 554 28. Kim, S., Chen, J., Cheng, T., Gindulyte, A., He, J., He, S., Li, Q., Shoemaker, B. A.,
555 Thiessen, P. A., Yu, B., Zaslavsky, L., Zhang, J., & Bolton, E. E. (2023). *PubChem 2023*
556 *update. Nucleic Acids Res.*, 51(D1), D1373–D1380.<https://doi.org/10.1093/nar/gkac956>

- 557 29. Lobanov, M.Y., Bogatyreva, N.S. & Galzitskaya, O.V. (2008). Radius of gyration as an
558 indicator of protein structure compactness. *Mol Biol* 42, pg 623–628
559 <https://doi.org/10.1134/S0026893308040195>
- 560 30. Maan, A. A., Nazir, A., Khan, M. K. I., Ahmad, T., Zia, R., Murid, M., & Abrar, M.
561 (2018). The therapeutic properties and applications of Aloe vera : A review. *Journal of*
562 *Herbal Medicine*, 12, 1–10. doi:10.1016/j.hermed.2018.01.002
- 563 31. Madeddu, F.; Di Martino, J.; Pieroni, M.; Del Buono, D.; Bottoni, P.; Botta, L.;
564 Castrignanò, T.; Saladino, R. (2022). Molecular docking and dynamics simulation revealed
565 the potential inhibitory activity of new drugs against human topoisomerase I receptor. *Int.*
566 *J. Mol. Sci.* 23, 14652. <https://doi.org/10.3390/ijms23231465>
- 567 32. Mahdizade Ari M, Dashtbin S, Ghasemi F, Shahroodian S, kiani P, Bafandeh E, Darbandi
568 T, Ghanavati R and Darbandi A (2023) Nitrofurantoin: properties and potential in treatment
569 of urinary tract infection: a narrative review. *Front. Cell. Infect. Microbiol.* 13:1148603.
570 doi: 10.3389/fcimb.2023.1148603
- 571 33. Mehdi Goudarzi, Saeedeh Ghafari, Masoumeh Navidinia and Hadi Azimi. (2018). Aloe
572 vera gel: effective therapeutic agent against extended-spectrum β -lactamase producing
573 escherichia coli isolated from patients with urinary tract infection in Tehran-Iran, *Journal*
574 *of Pure and Applied Microbiology*, Vol. 11(3), pg 1401-1408.
575 <https://dx.doi.org/10.22207/JPAM.11.3.22>
- 576 34. Mousavifar, L. Sarshar, M. Bridot, C. Scribano, D. Ambrosi, C. Palamara, A.T. Vergoten,
577 G. Roubinet, B. Landemarre, L. Bouckaert, J. et al. (2023). Insightful Improvement in the
578 Design of Potent Uropathogenic E. coli FimH Antagonists. *Pharmaceutics* 15,(2) pg 527.
579 doi: 10.3390/pharmaceutics15020527
- 580 35. Panche AN, Diwan AD, Chandra SR. (2016). Flavonoids: an overview. *J Nutr Sci.* vol 5:pg
581 47. doi: 10.1017/jns.2016.41.
- 582 36. Pettersen, E.F., Goddard, T.D., Huang, C.C., Couch, G.S., Greenblatt, D.M., Meng, E.C.,
583 and Ferrin, T.E. (2004). "UCSF Chimera A Visualization System for Exploratory Research
584 and Analysis." *J. Comput. Chem.* 25(13): pg 1605-1612. <https://doi.org/10.1002/jcc.20084>
- 585 37. Preman Geetika, Muskaan Mulani, Ayesha Bare, Khushboo Relan, Leebah Sayyed, Vikas
586 Jha, Kavita Pandey. (2022). Screening of phytochemicals for anti-Tubercular potential
587 using molecular docking approach. *J Tuberc.*; 5(1): pg 1030.
- 588 38. Rao P, Shukla A, Parmar P, Rawal RM, Patel B, Saraf M, Goswami D. (2020). Reckoning
589 a fungal metabolite, pyranonigrin A as a potential main protease (Mpro) inhibitor of novel
590 SARS-CoV-2 virus identified using docking and molecular dynamics simulation. *Biophys*
591 *Chem.* Vol 264 pg 106425. doi: 10.1016/j.bpc.2020.106425.
- 592 39. Salaria D, Rajan R, Mehta J, Awofisayo O, Olatomide A. Fadare, OA, Balvir K, Renato AC,
593 Shikha RC, Neha K, Eun HC, Nagendra KK. (2022). Phytoconstituents of traditional
594 Himalayan Herbs as potential inhibitors of Human Papillomavirus (HPV-18) for cervical
595 cancer treatment: An In silico Approach. *PLoS ONE* 17(3): pg 1-20.
596 <https://doi.org/10.1371/journal.pone.0265420>
- 597 40. Seifu WD, Gebissa AD. (2018). Prevalence and antibiotic susceptibility of uropathogens
598 from cases of urinary tract infections (UTI) in shashemene referral hospital, Ethiopia. *BMC*
599 *Infect Dis.* 18(1) pg 30. doi: 10.1186/s12879-017-2911-x.
- 600 41. Selvaraj A. Lakshmi, Raja M. B. Shafreen, Arumugam Priya & Karutha P. Shunmugiah.
601 (2021). Ethnomedicines of Indian origin for combating COVID-19 infection by hampering

- 602 the viral replication: using structure-based drug discovery approach, *J. of Biomolecular*
603 *Structure and Dynamics*, 39(13), pg 4594-4609, DOI: [10.1080/07391102.2020.1778537](https://doi.org/10.1080/07391102.2020.1778537)
- 604 42. S.B. Udugade, R.C Dojjad, B. V. Udugade. (2019). In silico evaluation of
605 pharmacokinetics, drug-likeness and medicinal chemistry friendliness of momordicin1: an
606 active chemical constituent of momordica charantia, *J Adv Sci Res*, 10 (3) gp 222-229.
- 607 43. Stanzione, F., Giangreco, I., & Cole, J. C. (2021). Use of molecular docking computational
608 tools in drug discovery. *Progress in Medicinal Chemistry*, 273–
609 343. doi:10.1016/bs.pmch.2021.01.004
- 610 44. Taj M, Shiza S, Anas S , Mohamed F. Alajmi, Afzal H, Asimul I, Faizan A and Imtaiyaz
611 H.(2020). Virtual screening approach to identify high-affinity inhibitors of serum and
612 glucocorticoid-regulated kinase 1 among bioactive natural products: combined molecular
613 docking and simulation studies, *MDPI Journal of molecules*. 13;25(4):823. doi:
614 10.3390/molecules25040823.
- 615 45. Terlizzi ME, Griboaldo G, Maffei ME. (2017). UroPathogenic *Escherichia coli* (UPEC)
616 Infections: Virulence Factors, Bladder Responses, Antibiotic, and Non-antibiotic
617 Antimicrobial Strategies. *Front Microbiol*. (8):1566. doi: 10.3389/fmicb.2017.01566.
- 618 46. Tomas Hansson; Chris Oostenbrink; WilfredF van Gunsteren (2002). Molecular dynamics
619 simulations. current opinion in structural biology, 12(2), 190–196. doi:10.1016/s0959-
620 440x(02)00308-1
- 621 47. Tripathi Kishua, Kumar T. Siva. (2010). Antibacterial activity of organometallic
622 complexes of cholic acid, *Dige J of Nanomat and Biostr*, Vol. 5, No 3 p. 763-770.
- 623 48. Van Der Spoel D, Lindahl E, Hess B, Groenhof G, Mark AE, Berendsen HJ (2005).
624 "GROMACS: fast, flexible, and free". *J Comput Chem*. 26 (16): pg 1701-1718.
625 doi:10.1002/jcc.20291
- 626 49. Veeresham C. (2012). Natural products derived from plants as a source of drugs. *J*
627 *Adv Pharm Technol Res*. 3(4): pg 200. doi: 10.4103/2231-4040.104709. PMID:
628 23378939; PMCID: PMC3560124.
- 629 50. Wade RC, Goodford PJ. (1989). The role of hydrogen-bonds in drug binding. *Prog Clin*
630 *Biol Res*.;289: pg 433-44. PMID: 2726808.
- 631 51. Wu, J.; Yu, T.T.; Kuppusamy, R.; Hassan, M.M.; Alghalayini, A.; Cranfield, C.G.;
632 Willcox, M.D.P.; Black, D.S.; Kumar, N. (2022). Cholic acid-based antimicrobial peptide
633 mimics as antibacterial agents. *Int. J. Mol. Sci*. vol 23, pg 4623. [https://](https://doi.org/10.3390/ijms23094623)
634 doi.org/10.3390/ijms23094623
- 635 52. Zagaglia, C.; Ammendolia, M.G.; Maurizi, L.; Nicoletti, M.; Longhi, C. (2022). Urinary
636 tract infections caused by uropathogenic escherichia coli strains—*New Strategies for an*
637 *old pathogen. microorganisms* 10, pg 1425. [https://doi.org/10.3390/](https://doi.org/10.3390/microorganisms10071425)
638 [microorganisms10071425](https://doi.org/10.3390/microorganisms10071425).
- 639
- 640
53. Tammana, T., Asif, M., Selina, A., Sazin, I., Sayeed, K. A. R., Jahangir, A. M., & Suvamoy, D.
(2015). Uropathogenic Analysis and Commonly Used Drug Sensitivity Patterns of the Pathogens
in Dhaka City, Bangladesh. *Journal of Advances in Medicine and Medical Research*, 11(1), 1–8.
<https://doi.org/10.9734/BJMMR/2016/21365>
54. Iroha , G. O., Adejumo , T. O., Osuntokun , O. T., & Coker , M. E. (2023). Plasmid-encoded
Antibiotic Resistant Bacteria of Surgical Wound Isolates from Three Hospitals in Akoko Land.

Journal of Advances in Medical and Pharmaceutical Sciences, 25(5), 43–64.

<https://doi.org/10.9734/jamps/2023/v25i5620>

55. Raksha R, Srinivasa H, Macaden RS. Occurrence and characterisation of uropathogenic *Escherichia coli* in urinary tract infections. Indian journal of medical microbiology. 2003 Apr 1;21(2):102-7.

UNDER PEER REVIEW